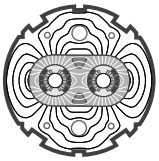

LHC Project Note 78 / 97

January 18, 1997
zazula@mail.cern.ch

On Graphite Transformations at High Temperature and Pressure Induced by Absorption of the LHC Beam

Jan M. Zazula

CERN-SL/BT(TA)

Keywords:

Summary

The central part of the graphite core of the LHC beam dump will be subjected for short time periods to very high internal temperature and pressure, induced by energy deposited by particle cascades. Extreme concentration of absorbed power could occur for an accidental absorption of undiluted 7 TeV/c proton beam of 4 mm diameter, at the maximum design intensity of $4.8{\cdot}10^{14}$ protons, in an 86 μs pulse. Analogy of such conditions is found, and comparison is made with recently reported pulsed laser heating experiments with graphite. Analysis of the actually established phase diagram (p, T) of carbon leads to a conclusion that because of high pressure, generated by the impact (shock) character of heat generation load, the graphite in the dump core would rather melt than vaporise. Incidental interception of an undiluted beam will most probably lead to a local transient phase change to the liquid carbon state (observable in the reviewed experiments) allowing further safe absorption of the cascade energy, and followed by condensation to solid forms of carbon (with a possible fraction of diamond). Expected temperature and pressure levels are estimated by means of the particle shower simulations, and the subsequent transient non-linear coupled thermo-mechanical finite element analysis with incorporated melting. They confirm, nevertheless, that with the designed beam sweeping system operational, the dump core graphite will remain in conditions favourable for the solid state.

1 Introduction

1.1 Phase diagram of carbon

A favourable material for the LHC beam dump core [1, 2, 3] is carbon, in the form of graphite [4, 5, 6, 7]. The phase diagram (p, T) of carbon was controversial for many years (see, *e.g.*, [8, 9, 10, 11, 12, 13, 14]), and only recently well established experimentally - up to now, within the temperature range up to about 10 000 K [1] and the pressure range up to about 100 Gpa; the higher region being still poorly understood. The diagram is shown in Figure 1, as based on [10, 11].

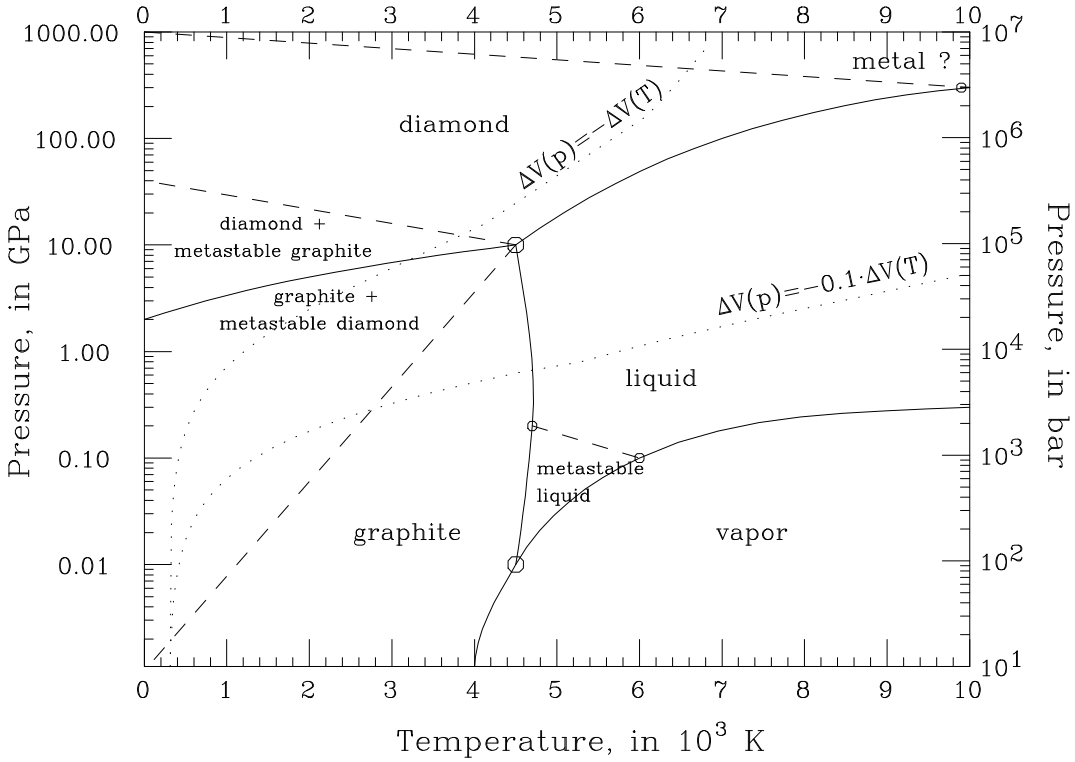

Figure 1: Phase diagram of carbon. See Section 4 for explanation of transformations defined by dotted lines.

There are at least two stable solid phases of carbon: from the structural point of view, graphite represents a crystalline hexagonal form, and diamond a tetrahedral form. Both these forms can exist in the same quite wide range of thermodynamic conditions; however, graphite can be transformed to diamond only at very high pressures, above 10 GPa. The intermediate meta-stable solid phases like carbyne and chaoite are discussed for several years [8]. Evidence for a solid-to-solid phase transformation from diamond to a metallic state (Solid III), possibly cubic, is described [15] at extreme high pressure ($>$100 GPa).

It is well known that at ambient pressure graphite will sublimate when heated rather than melt. The pressure of gaseous carbon is, however, relatively low, and at sufficient temperature and pressure graphite will melt rather than vaporise. Two liquid phases were deduced from experiments: one metallic and the other semi-metallic. The two triple-points are estimated to lie at temperatures

[1] Molecular dynamics simulations can be extended at least to 20 000 K limit

between 4300-4700 K, and pressures between 0.01 GPa (graphite - vapour -liquid) and 10 GPa (graphite - liquid - diamond).

1.2 Thermo-dynamical impact of the LHC beam

The principal problem discussed in this note is how the graphite of LHC beam dump core will evolve on this diagram, after interception of the LHC beam at highest energies and intensities – in normal operating (swept beam) or accidental (undiluted beam) conditions.

High energy beam protons are absorbed by developing the hadronic and electron-photon cascades, of few meters longitudinal extension, and of high concentration on beam axis. The shower products propagate, interact, decay, slow down, are absorbed or escape in a time as short as tens of nanoseconds (comparable with the LHC bunch spacing), finally dissipating their energy by internal generation of heat and pressure. These loads acts as a pulse of about 10^{-4} s length, the time scale required for abort of the LHC beam. High spatial density and gradient of the loads are essential, and even more their short duration – heating time being characteristic rather for elastic wave propagation (microseconds) than for heat conduction (milliseconds). Effects usually persisting for time much longer than beam interception period, are temperature and pressure (more generally, stress) rise, shock waves, structure deformations, and possible phase transitions. It is well known that a highly localised heat pulse, sufficiently short to suppress thermal conduction and thermal dilatation, can create extremely high temperature and pressure. Therefore, the literature concerning the pulsed heating of graphite is reviewed in the next Section.

2 Review of experiments

Graphite exhibits elastic behaviour and even improves its mechanical strength up to the temperature of about 2500 K. Measured changes in ultrasonic velocity in graphite after high temperature creep shows marked plasticity at temperatures above 2200 K [16]. From the standpoint of thermodynamics, melting is a phase transition of the first kind, with an abrupt enthalpy change constituting the heat of melting. Therefore, any experimental proof of melting is associated with direct recording of the temperature dependence of enthalpy in the neighbourhood of a melting point.

Pulsed heating of carbon materials was studied experimentally by transient electrical resistance and arc discharge techniques, in millisecond and microsecond time regime (see, *e.g.*, [17, 18]), and by pulsed laser heating, in microsecond, nanosecond and picosecond time regime (see, *e.g.*, [11, 19, 20]). Both kind of experiments recorded significant changes in the material properties (density, electrical and thermal conductivity, reflectivity, *etc.*) within the range 4000-5000 K, interpreted as a phase change to a liquid state. The results of graphite irradiation by lasers suggest [11] that there is at least a small range of temperatures for which liquid carbon can exist at pressure as low as 0.01 GPa. The phase boundaries between graphite and liquid were investigated experimentally and defined fairly well.

With laser melting experiments, the emitted light power and time length of the pulse can be controlled, and the temperature of a sample can be monitored by means of the emitted thermal radiation (the radiated power being, however, much smaller than laser power incident on the sample). The laser-induced damage in crystalline symmetry can be seen, *e.g.*, by line broadening in Raman scattering spectroscopy [21]; the micro-structure of the disordered layers was also examined by

transmission electron microscopy [22]. The electronic structure of the new phase is found to be intermediate between graphite and diamond.

An important and representative experimental work on pulsed-laser melting of graphite was performed in the previous decade in the Massachusetts Institute of Technology and Bell Laboratories [11, 19]. Typical laser pulses are Gaussian in time with a full width at half maximum of 30 ns [19], so the thermal energy is coupled into the graphite lattice in a time period small enough to eliminate the contribution of sublimation process that has been observed to occur with slower heating techniques. The laser light power densities of order 10^8 W/cm^2, nearly all deposited into a thin layer ($\sim$1000 Å) near the front surface, over a peak area $\sim$0.25 cm^2, can yield local specimen temperature in excess of 5000 K [11]. The thickness of amorphous layer increases with incident pulse fluence from a threshold about 0.6 J/cm^2, eventually saturating at an energy density of 1.8 J/cm^2 [19]. The same authors studied also re-growth of graphite as the molten carbon cools; a residence time of $\sim$150 ns is estimated for annealing of graphite. The samples recovered after solidification of directly melted graphite were found to consist of a hybrid mixture of graphite and diamond [23].

Irradiations with tens of picosecond laser pulses [20] provide observations in a time shorter than that required for the hot surface layer to evaporate (distorting the emissivity measurements), but yet long enough for complete thermalisation between the electron gas and lattice. In this case the surface temperature is so high that the equilibrium vapour density becomes comparable to the original solid density, and the plasma effects become observable. These experiments indicate the ultrafast transformation to the liquid phase already at a laser fluence of 0.14 J/cm^2, and the melting threshold of $\sim$3900 K.

Transition from graphite-like to solid diamond-like behaviour is another phase change in carbon, observed at pressures in excess of 10 GPa and temperatures up to 5000 K. The complementary mechanical shock compression experiments were performed in the Los Alamos [14, 24] and Lawrence Livermore [15, 25] National Laboratories. Initially shocked graphite becomes an insulator at higher pressures, indicating extremely rapid (τ <10 ns) collapse into the diamond phase. The diamond cristallines are recovered from graphite samples compressed by shock waves, *e.g.*, to 30 GPa applied for 1 μs. Synthesis of diamond is successfully carried out by applying a thermal quenching technique (see, *e.g.*, [26]); sufficient cooling rate by copper sandwiches embedded into a thin graphite plate can almost suppress re-graphitisation. Such conditions favour the formation of meta-stable phases [22, 29]. At (p, T)=(83 GPa, 3000 K) more than 90% of the sample is transformed to cubic diamond; however, at (26 GPa, 600 K) the graphite remains only deformed mechanically. Melting of the diamond to a liquid carbon was also investigated [27, 30], with an upper bound of the diamond T$_m$ $\approx$8000 K.

3 Liquid carbon

A melting point of high purity graphite was found at temperature T$_m$=4700$\pm$80 K [2]. The recommended value of latent heat of graphite is ΔH$_m$=105$\pm$15 kJ/mol. This absorbs quite substantial amount of energy, comparable with that necessary to heat 1 mol from room temperature to the melting point (see Figure 2, with logarithmic energy scale). Diamond has a similar heat of fusion, $\sim$125$\pm$15 kJ/mol. However, the measured enthalpy of transformation between diamond and

[2] The highest value of 5080 K was reported by the Russian group [17]

graphite is only $\sim$2 kJ/mol.

A controversial point [10, 28, 31] is that liquid carbon had been found to be an electric insulator at low pressures (p$<$0.02 GPa), but conductive metallic liquid at pressures above 1 GPa; these results seem to obviate the need for having two distinct liquid phases. The density of semi-metallic liquid at the triple point is estimated to be 1.3$\sim$1.5 g/cm^3 [30], and the closely-packed metallic liquid can reach at high pressures $\sim$2.7 g/cm^3 [11], just between the graphite (1.7$\sim$2.2 g/cm^3) and diamond density ($\sim$3.5 g/cm^3).

4 Pressure conditions created by pulsed heating

The pressure conditions necessary for graphite melting focused a theoretical debate (see, *e.g.*, [13, 10, 30, 32]). In particular, there is no universal agreement whether or not liquid carbon can exist at pressures below 100 bar.

Estimation of pressure must be based on measurements or theoretical extrapolation of mechanical properties of carbon up to temperatures above the melting point, This is accomplished by using the parametrised experimental data on molar volume V of carbon as a function of temperature and pressure [13], and its derivatives:

$$\alpha_V = \frac{1}{V_o}\left(\frac{\partial V}{\partial T}\right)_p \quad ; \quad \kappa = -\frac{1}{V_o}\left(\frac{\partial V}{\partial p}\right)_T \tag{1}$$

which are the volume thermal expansion coefficient α_V and compressibility κ; $V_o = V(p_o, T_o)$ is the reference molar volume in [cm^3] (usually, at room temperature T_o and atmospheric pressure p_o); related to the respective mass density ρ_o in [g/cm^3] by $V_o = M/\rho_o$, where M is one mole in grammes.

The data on molar volume, are presented and interpreted in [10, 13]. With free boundaries and after sufficiently long time, the effect of temperature rise (at constant pressure) is thermal expansion ($\Delta\, V > 0$), or reduction in density. The effect of external pressure (at constant temperature) is a compression ($\Delta\, V < 0$), or density rise. Thus with fixed boundaries, an effect of a temperature rise must be an internal pressure.

The maximum level of thermal pressure is significantly affected by the time regime of heating. Graphite can expand with a sound velocity of about 2.3 mm/μs, thus the pressure persists for a time (depending on system dimensions) until the thermal dilatation is completed. Thermal shock is generated by a heat pulse so intense and short that the structure has no time to expand, as with an external boundary being temporarily fixed. In the extreme case of iso-volumetric process ($\Delta\, V = 0$) the total rise of molar volume due to thermal expansion is suppressed by an equivalent thermal pressure:

$$\Delta\, V(p_o, T_o + \Delta\, T) = -\Delta\, V(p_o + \Delta\, p, T_o) \tag{2}$$

The formula above determines pressure rise $\Delta\, p$ generated by temperature rise $\Delta\, T$ at constant volume, or for an infinitely short time. The (p, T) curve defined by this equation is shown for graphite in Figure 1, as the upper dotted line. It can be seen that an instantaneous temperature rise up to, *e.g.*, melting threshold, would be able to create an enormous pressure of 10-100 GPa, probably sufficient to transform graphite into diamond instead of liquid. However, instantaneous heating is a far too idealistic condition, possible to approach approximately only in ultra-fast (picosecond)

laser melting experiments [10]. The microsecond regime of "slow" experiments is rather attributed [10] to a pressure range 0.2-0.5 GPa, re-compensating only unrealised 10% of the maximum thermal dilatation (the lower dotted curve in Figure 1); this is sufficient, nevertheless, to exceed the graphite melting line.

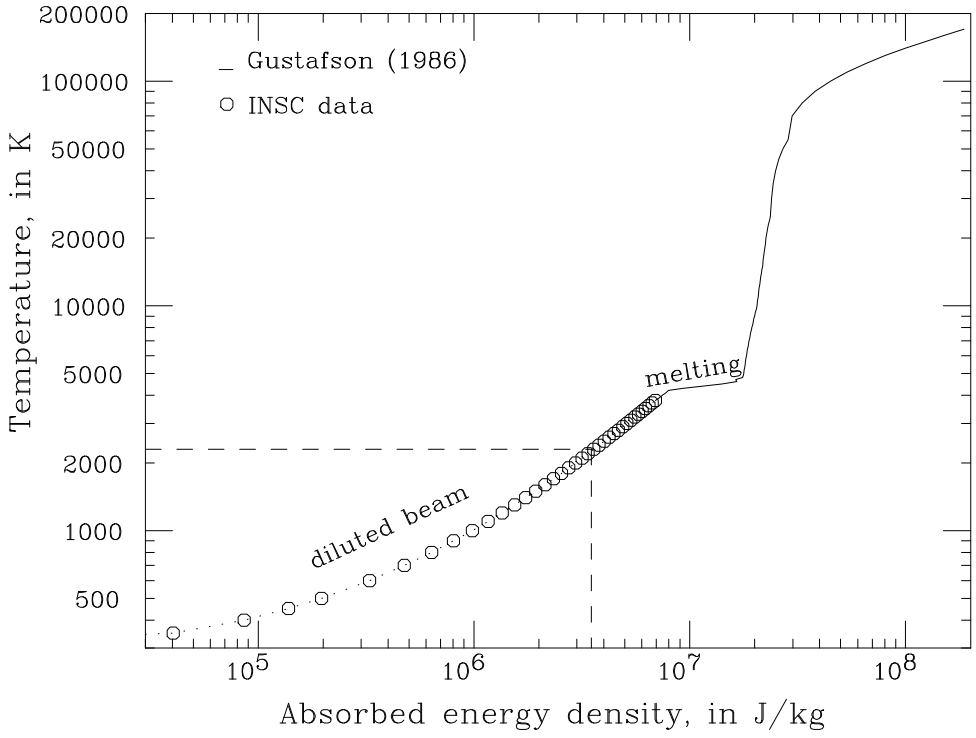

Figure 2: Temperature versus energy density absorbed in graphite and liquid carbon.

5 Comparison of laser heating with LHC beam heating

Experimentally established data on latent heat and specific heat of the liquid carbon enable to extend the enthalpy versus temperature curve to high temperatures and energy densities. It is worth noting that for heating at an approximately constant volume the internal energy U (not including mechanical work of expansion) is a more appropriate thermo-dynamic potential than the enthalpy [38]. It can be expressed as a temperature integral:

$$dU(\Delta T) = \int_{T_o}^{T_o+\Delta T} dT\ \rho\, C_V(T) \tag{3}$$

of specific heat at constant volume C_V, where $\rho = const$ is the material density. For absorption of a high energy cascade, the internal energy is incremented by the deposited energy density. The instantaneous (iso-volumetric) temperature rise versus absorbed energy is shown in Figure 2; the low energy INSC data [39] are quite consistent with a high temperature parametrisation developed in course of this study (see Section 6.1) on the basis of [11, 13]. The latent heat was uniformly distributed over the melting region 4300-4700 K, as an additional component of the temperature-integrated specific heat.

The beam sweeping system, addressed to normal operating conditions of the LHC beam dump, is designed not to exceed the optimal temperature range of graphite utilisation, up to 2300^{o}C . The cascade simulations [2] with FLUKA program [41] show, however, that in highly improbable incidental absorption of undiluted beam at maximum intensity the local energy concentration can reach level higher than 10^8 J/kg, at the end of 86 μs pulse. This leads to a significant excess of the graphite phase transformation temperature. For infinitely short heat pulse of this intensity (an assumption fairly too pessimistic for 86 μs absorption period) temperature could locally rise even above 100 000 K which leads apparently to the plasma conditions. In any case, the peak power density $\sim$1 GW/cm^3 deposited from maximum intensity undiluted LHC beam ($\sim 10^5$ J/cm^3 per $\sim 10^{-4}$ s) is one order of magnitude higher than the typical 10^8 W/cm^3 high power density of the laser light (if uniformly extended in specimen depth). Thus the energy and temperature conditions of the described carbon melting experiments are already met by a partially swept LHC beam, although they are far too high to be reached for the usual (swept) beam abort.

The laser irradiated area ($\sim$1 cm^2) in the experiments is quite similar to the lateral section of the hottest region in the energetic particle cascade. The most important difference is that contrary to the laser beam, effective only on a very thin front surface layer of the specimen (in most cases in contact with vacuum), the high energy hadronic and electro-magnetic cascade need a depth range of rather meters than micrometers to develop, so they deposit energy internally in a large part of the graphite volume, the upstream face being remarkably less heated than the maximum, at about 2 m. This again acts in favour of melting rather than vaporisation, since most of the material submitted to intense heat generation has no access to a free surface of sublimation (other than several vacuum pumping channels in the core). Moreover, a high stress (in solid) or pressure (in liquid) is more likely to concentrate in and will be more difficult to release from the central parts of the core.

Verifying if the pressure criterion for carbon melting can be fulfilled under absorption of the LHC beam is the remaining, most difficult part of this study. Assuming a very high pressure created by instantaneous temperature rise, or by temperature rise at constant volume (see upper dotted curve in Figure 1), would be of course a fairly unrealistic approach, except perhaps of relatively low temperatures. However, the laser pulse duration applied in some of the experiments compares well to the time for absorbing cascades induced by a single LHC bunch (tens of nanoseconds), by a bunch train (microseconds), or, in other experiments, to the overall beam abort time (tens of microseconds). Thus, intuitively, the pressure in a high energy proton beam absorber must not be much different than that created by 1-100 μs laser pulses, deduced to be $\sim$0.1 GPa, because of the similar intensity and time characteristics of the heating. However, the problem is more subtle: one can consider temperature rise being either fast or slow only in context of system dimensions. It is, *e.g.*, well established [37] that the maximum stress in a uniformly heated freely suspended thin elastic rod is reduced (with respect to a sudden heating) by a factor determined by the ratio of the longitudinal sound propagation duration to the heating period. Due to axial concentration of the cascade, the high energy beam heating is quite similar to the microsecond laser pulse heating in radial direction (longer than time required for transverse sound waves to reach the block edge) – but quite different in longitudinal direction (and rather prompt), since the deformation waves cannot propagate (with speed of sound) as far as up to 700 cm block depth, partially releasing the longitudinal stress before 86 μs. This can be used as an argument for a segmented structure of the dump core, to suppress thermal shock. Nevertheless, the pressure at any point must be significantly dependent on localisation (spatial distribution of the load being far from uniform) and on time, even in microsecond scale (due to dynamic stress waves).

6 Finite element analysis

If the material properties are determined with some certitude, the finite element ($\mathcal{FE}$) method seems to be the best suited calculation tool. In principle, it enables the observation of volume variation (by means of strain) in any particular element at any particular period, and thus to determine the mean pressure by means of stress (see next Section). It is not intent of this work to perform detailed studies of spatial distribution and time evolution of the temperature and stress (as is separately performed for the operational sweep conditions, in the third part of the LHC beam dump design study), but to examine what would be the most probable thermo-dynamical phase state of any piece of the core graphite, if incidentally submitted to the extreme conditions (maximum beam intensity and total or partial sweep failure).

The $\mathcal{FE}$ calculations were performed with the use of ANSYS system [40]. The nonlinear transient coupled thermal-structural analysis options were applied. No hydro-dynamic effects (liquid carbon flow) were simulated, but mass transport seems to be quite a slow process, occurring only in a relatively small volume in the central part of the core.

6.1 Material properties

A disordered isotropic graphite is assumed as the material of the dump core. It is characterised by initial density, 1.75 g/cm^3 for the solid state (at 300 K and 1 bar), and 1.5 g/cm^3 for the liquid (at 4700 k and 10^5 bar); evolution of the material density with variable pressure and temperature can be only obtained from the output of $\mathcal{FE}$ analysis. The "low" temperature graphite properties were taken from [6, 33, 34, 35, 36].

Melted carbon is assumed to be an ideal metallic liquid; the specific heat and thermal conductivity are well modelled (see, *e.g.*, [11, 13, 28]) with a free electron Fermi gas model, assuming 4 electrons per atom. Its elastic properties are determined by only one temperature-dependent parameter which is volumetric compressibility κ (see Equation 1). The elastic modulus E can be derived [38] by using the relation:

$$E = 3\,(1 - 2\,\nu)\,\frac{1}{\kappa} \tag{4}$$

where the Poisson's ratio $\nu = 0$ is taken for liquid.

For calculation of thermal deformations with the ANSYS system, the assumed bulk densities of the solid and liquid are referred to the (initially) constant volume, while most of the thermodynamic data are tabulated or parametrised at constant pressure; the difference can be significant at high temperatures. The material properties were therefore transformed, according to Landau [38]:

$$C_V = C_p - \frac{\alpha^2\,V\,T}{\kappa} \tag{5a}$$

$$E_V = \frac{E_p}{1-\eta} \quad ; \quad \mu_V = \frac{\mu_p + \eta}{1-\eta} \tag{5b}$$

where

$$\eta = E_p \frac{\alpha^2\,V\,T}{9\,C_p} \tag{5c}$$

The assumed or calculated material properties of carbon: linear expansion coefficient $\alpha_l = 1/3\,\alpha_V$, elastic modulus E, specific heat C_V and thermal conductivity k, are shown in Figure 3 as a function of temperature. The enthalpy (internal energy) versus temperature (derived from specific heat C_V and heat of fusion H_m) has already been presented in Figure 2 of this note. These figures are fairly consistent with the data assumed for the LHC beam dump design study [2, 3].

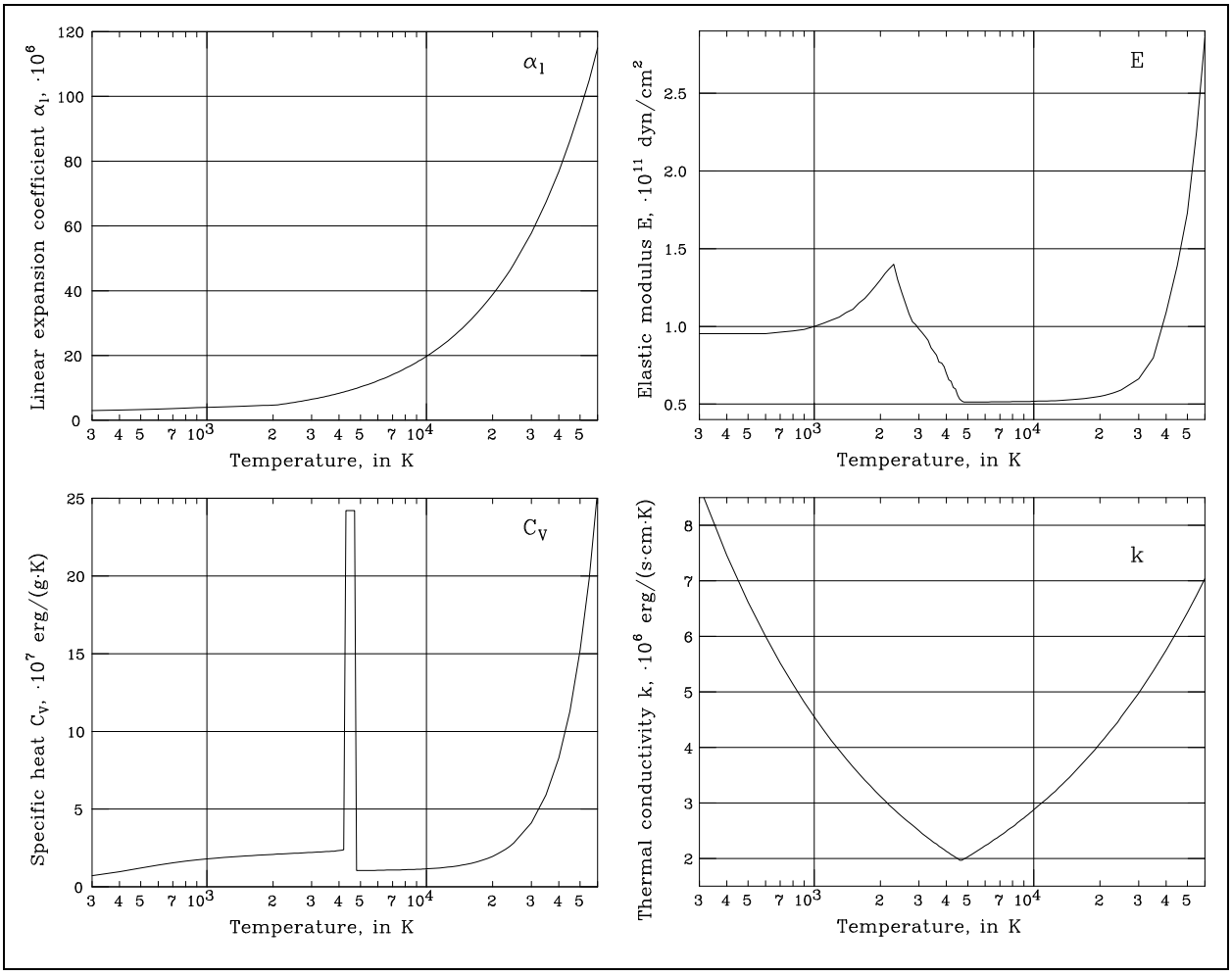

Figure 3: The temperature-dependent material properties of carbon: linear expansion coefficient α_l, elastic modulus E, specific heat C_V and thermal conductivity k (the cgs units are used).

6.2 Model and loads

The central part of dump core can be roughly modelled as a homogeneous cylindrical block of graphite (undiluted beam being the azimuthal symmetry axis), of 30 cm radius and 700 cm length; the aluminium container and other external parts of the dump (base plate, shielding) are neglected for the purpose of this study. The $\mathcal{FE}$model is based on the 2-dimensional (axi-symmetrical) first-order (4 node) coupled thermo-mechanical elements, of temperature and structural displacement degrees of freedom. The model was meshed using 20 radial divisions (compressed with a factor

5:1 around beam axis), and 50 longitudinal divisions (upstream compressed with a factor 3:1). A uniform initial temperature 300 K is assumed, and the system is simulated only for the first 86 μs beam interception period when the thermal loads are active, in time sub-steps about 1 μs. In such a large system the outer shape and boundary conditions do not play significant rule for such a short time, so all the external surfaces were assumed adiabatic and free of constraints.

The thermal load input for each elemental node was the internal heat generation rate, taken as the density of energy deposited from particle cascades, normalised to the total number of protons in the maximum intensity beam, and expressed per unit time (by dividing by beam abort period). Thus the loads are uniformly distributed in time for the first 86 μs (the time pattern of bunches and trains being replaced by continuous approximation), and then they vanish. A correction for liquid density slightly different than for solid was performed above the melting temperature, assuming constant energy deposition per unit mass of carbon. The spatial distribution of the loads is due to the cascades induced by the undiluted LHC beam, of about 4 mm diameter; it is transferred from the output of FLUKA shower simulation program (see [42]), assuming all bunches incident at the same place. It is worth recalling here (see [2]) that in this case the energy density has longitudinal maximum at about 185 cm depth; at this depth more than 90% of the laterally-integrated energy distribution is contained within 5 cm radius around undiluted beam axis.

6.3 Results

The output of the $\mathcal{FE}$solution are nodal temperatures and displacements, and the components of the strain and stress tensors in each element, as a function of time. However, only the extreme results that occurs at the end of the heating period has been stored and are analysed here.

The mean hydrostatic pressure p in an element can be derived from an equivalent relative change in volume:

$$\frac{\Delta\, V}{V_o} = -\kappa\; p \tag{6}$$

where the volume change can be obtained from the sum of diagonal elements $u_{ii}(i = x, y, z)$ of the strain tensor:

$$\frac{\Delta\, V}{V_o} = \sum_i\; u_{ii} \tag{7}$$

which is invariant. Using on the right side of this formula the stress - strain relation for the diagonal tensor elements:

$$\sum_i\; u_{ii} = \frac{1-2\nu}{E} \sum_i\; \sigma_{ii} = \frac{\kappa}{3} \sum_i\; \sigma_{ii} \tag{8}$$

and comparing with equation (6), the sum of diagonal stress components σ_{ii} in any coordinate system, calculated by ANSYS, can be used to estimate the mean hydrostatic pressure as, *e.g.*, :

$$p = -\frac{1}{3}\; (\sigma_{xx} + \sigma_{yy} + \sigma_{zz}) \tag{9}$$

The results are presented in Figure 4 by means of the (p, T) diagram. Each elemental pair of temperature and pressure, with no respect to element position, is shown as one vertical cross; it is obvious that elements showing the highest values of temperature and pressure are those localised close to beam axis and at depth of cascade maximum. Nevertheless, many different elements found

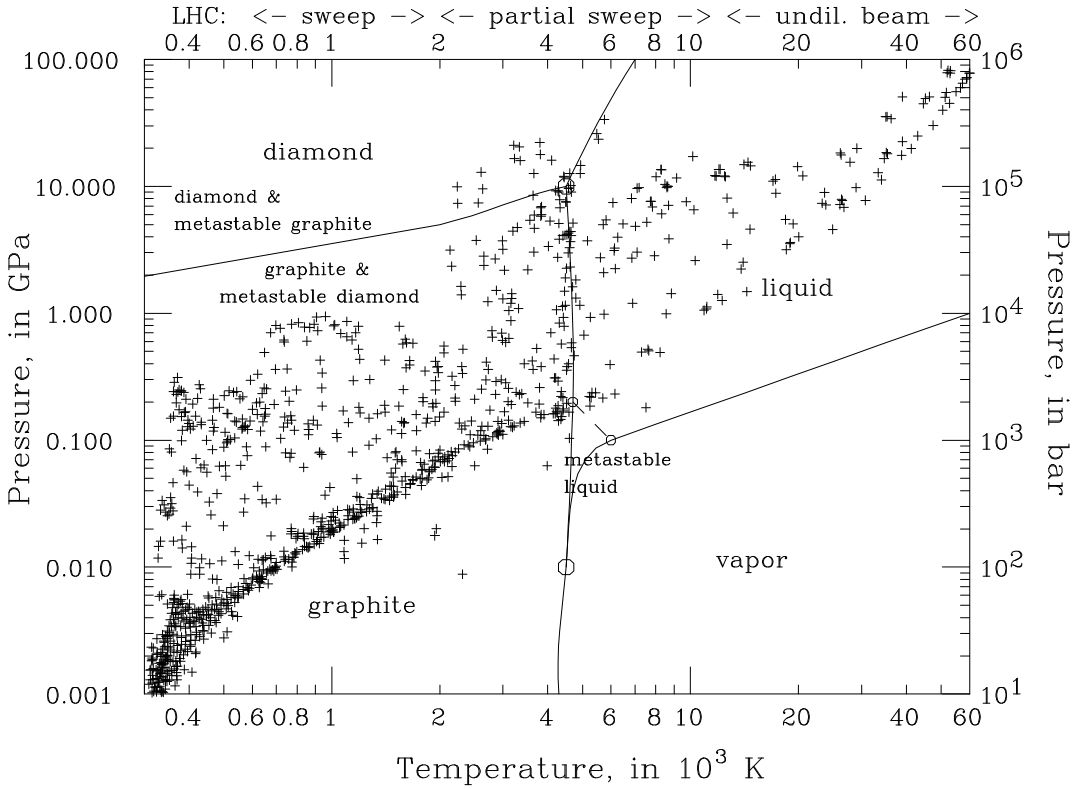

Figure 4: Temperatures and pressures expected in the LHC dump core, under operating or accidental conditions, shown on the phase diagram of carbon.

at the same temperature need not necessarily reach the same pressure. This is explained by the fact that in reality there are two pressure components: only the first one is that of directly thermal origin, uniquely defined by temperature; the second component is, however, the pressure of neighbouring elements, *e.g.*, propagating by dynamic stress waves with the speed of sound. Such waves can traverse several cm in graphite during the 86 μs period, and pressurise "cold" elements, those with internal heat generation not sufficient for substantial temperature rise. Therefore, already after a few microseconds of heating the pressure fails to be strictly proportional or uniquely related to the temperature field or its gradient.

The (p, T) phase boundaries in carbon are also shown in the same Figure. It can now be seen that for temperatures up to $\leq$2300 K, corresponding to energy density diluted by the beam sweeping system (although the incident bunch distribution along the sweep profile is not modelled here in detail), pressures hardly reach the level of 1 GPa, and the graphite remains well in the solid state. Higher temperatures more likely generate large pressure variations; in rare cases even the conditions for transition into diamond seem to be realised at about 2500-4000 K. However, in this temperature range the graphite shows rather plastic behaviour which was not modelled in detail (except of a substantial suppression of the elastic modulus), so the extreme results for pressure in solid, obtained under assumption of elasticity, might be too high; this temperature range might still require more appropriate strain-stress relation model, more precise material data and careful investigation.

The 4500 temperature threshold is mostly met on the graphite-liquid (p, T) boundary; at such high temperatures, pressures as low as vapour pressure are rather improbable. This simply proves that the graphite of dump core, submitted to undiluted or only partially swept maximum intensity

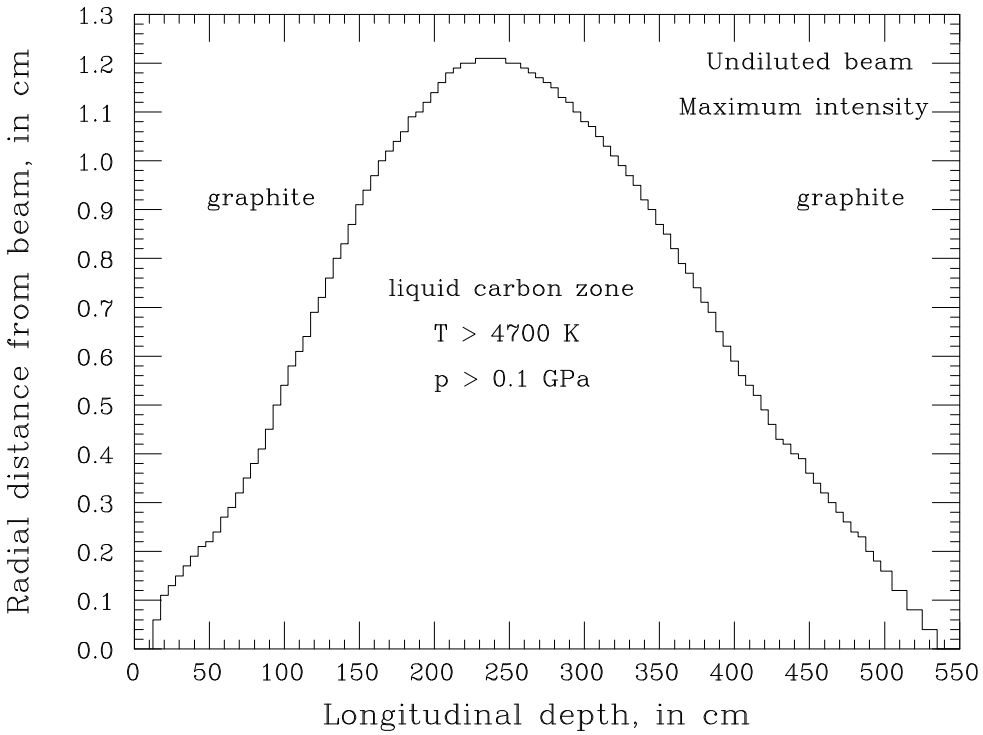

Figure 5: Maximum radii of liquid carbon zone versus depth, for accidental absorption of undiluted LHC beam at maximum intensity.

proton beam, is more likely to melt than sublimate.

The last question addressed in this note is how far the liquid zone can be extended radially and longitudinally. Figure 5 presents the (r, z) coordinates where the melting point is exceeded; only the maximum radius of the liquid region is shown for each z. The plot shows that after 86 μs absorption of maximum intensity undiluted beam, the liquid carbon region, of maximum diameter about 2.5 cm around beam axis, could possibly extend in depth between 15 and 540 cm. The question can be raised whether the external solid graphite structure contained in the aluminium frame would be strong enough to sustain an extremely high internal pressure. However, the solid layer directly surrounding the pressurised liquid would be hot enough to become a plastic material, and plastic deformation seems to be safer than the elastic one, for the solid-liquid contact zone.

7 Conclusions

The worst imaginable consequence of incidental absorption of maximum intensity undiluted LHC beam could eventually be the prompt (in few or several microseconds) piercing of a hole in the dump structure, filled only by rapidly expanding carbon gas. In this case, the carbon vapour would not be a sufficiently dense medium for developing compact particle cascades and absorbing the required amount of energy, so that an almost undiluted beam would finally touch the downstream heavy material absorbers (Al and Fe) or even ground, with extremely dangerous concentrations of deposited energy and induced radioactivity.

The conclusion of this study, *i.e.*, melting rather than vaporising of some central part of the

graphite core in accidental conditions, leads to a less pessimistic scenario. Firstly, absorption of the substantial latent heat necessary for phase transition, at almost constant melting temperature, is an additional and useful barrier for temperature rise. Even if this barrier is locally forced by the maximum deposited energy density, a small amount of a hot dense liquid inside is still a relatively safe state for the dump core: the liquid carbon still retains properties required to develop and safely absorb hadronic and electron-photon showers. It can even better endure high pressure than the solid graphite, and no reason is seen why it could not be heated even up to tens of thousand K. The compressed liquid phase, totally surrounded by the outer solid region (with a partially plastic hot layer inside), would have no means of escape through an external boundary, which reduces the risk of explosion or implosion. The plastic behaviour of the solid near melting point can also be useful for amortising contact with the pressurised liquid, and for dissipating the energy of dynamic stress waves. Moreover, after the heat generation disappears, the liquid phase could possibly re-condensate again to the solid forms of carbon, as it was observed in laser melting experiments. Thus the damage in the central part of core would be, at least partially, recuperated. This confirms that graphite, at high temperatures and pressures, is an excellent and safe material for the LHC beam dump core.

Acknowledgements

I would like to thank Serge Péraire, Eberhard Weisse, Murray Ross and Graham Stevenson for encouraging me to make this study, for continuous background in all aspects of the LHC project, and for a lot of time spent together in discussions. The scientific information services at CERN are appreciated for their efficiency in making available the literature from many physical disciplines, sometimes quite exotic from elementary particle research.

References

[1] P. Lefèvre and T. Petterson (Eds.), "The Large Hadron Collider: Conceptual Design", CERN AC/95–05 (LHC), Geneva (October 1995).

[2] J.M. Zazula and S. Péraire, "LHC Beam Dump Design Study; Part I: Simulations of energy deposition by particle cascades; implications for the dump core and beam sweeping system", LHC Project Report 80 / 96, CERN, Geneva (October 1996).

[3] S. Péraire and J.M. Zazula, "LHC Beam Dump Design Study; Part II: Thermal analysis; implications for abort repetition and cooling system", LHC Project Report 87 / 96, CERN, Geneva (December 1996).

[4] R.E. Nightingale, Ed., "Nuclear Graphite", Academic Press, New York (1962).

[5] C.L. Mantell, "Carbon and Graphite Handbook", J. Willey & Sons, New York (1968).

[6] W.N. Reynolds, "Physical Properties of Graphite", New York, Elsevier (1968).

[7] B.T. Kelly, "Physics of graphite", Applied Science Publishers, LTD, London and New Jersey (1981).

[8] A.G. Whittaker, "Carbon: A New View of Its High-Temperature Behaviour", Science 200, 763 (1978).

[9] A.G. Whittaker, "The Controversial Carbon Solid-Liquid-Vapour Triple Point", Nature 276, 695 (1978).

[10] F.P. Bundy, "Pressure-Temperature Phase Diagram of Elemental Carbons", Physica A 156, 169 (1989).

[11] J. Steinback *et al.*, "A Model for Pulsed Laser Melting of Graphite", J. Appl. Phys. 58 (11), 4374 (1985).

[12] D.A. Young and R. Grover, "Theory of the Carbon Phase Diagram at High Temperatures and Pressures", in *Shock Waves in Condensed Matter 1987 (S.C Schmidt and N.C Holmes, Eds.)*, pp. 131-34, Elsevier Sci. Publ. B.V. (1988).

[13] P. Gustafson, "An Evaluation of the Thermodynamic Properties and the (p, T) Phase Diagram of Carbon", Carbon 24, 169 (1986).

[14] A.C. Mitchell, J.W. Shaner and R.N. Keeler, "The Use of Electrical Conductivity Experiments to Study the Phase Diagram of Carbon", Physica B 139 & 140, 386 (1986).

[15] W.H. Gust, "Phase Transition and Shock Compression Parameters to 120 GPa for Three Types of Graphite and for Amorphous Carbon", Phys. Rev. B 22 (10), 4744 (1980).

[16] M. Narisawa, M. Adachi and I. Souma, "Changes in Ultrasonic Velocity in Graphite After High Temperature Creep", Carbon 30, 815 (1992).

[17] A.V. Baitin *et al.*, "The Melting Point and Optical Properties of Solid and Liquid Carbon at Pressures up to 2 kbar", High Temp.-Press. 21, 157 (1990).

[18] M.A. Scheindlin and V.N. Senchenko, "Eksperimentalnoje issliedowanije tiermodynamitscheskich swoistw grafita w okriesnosti totschki plawlienija", Dokl. Akad. Nauk S.S.S.R 298 (6), 1383 (1988).

[19] T. Venkatesan *et al.*, "Measurement of Thermodynamic Parameters of Graphite by Pulsed-Laser Melting and Ion Channelling", Phys. Rev. Lett. 53 (4), 360 (1984).

[20] A.M. Malvezzi, N. Bloenberger and C.Y. Huang, "Time-Resolved Picosecond Optical Measurement of Laser-Excited Graphite", Phys. Rev. Lett. 57 (1), 988 (1986).

[21] M. Hanfland, H.Beister and K. Syassen, "Graphite Under Pressure: Equation of State and First-Order Raman modes", Phys. Rev. B 39 (17), 12598 (1989).

[22] F.J.M. Rietmeijer, "A Transmission Electron Microscope Study of Experimentally Shocked Pregraphitic Carbon", Carbon 33, 827 (1995).

[23] M.S. Weathers and W.A Bassett, "Melting of Carbon at 50 to 300 kbar", Phys. Chem. Minerals, 15, 105 (1987).

[24] J.W. Shaner *et al.*, "Sound Velocity of Carbon at High Pressures", J. de Phys. 45 (11), C8-235 (1984).

[25] F.H. Ree, M. Van Thiel and D. Calef, "Stability of Graphitic and Diamond Clusters and Their Transformation Rates Under High Pressure and High Temperature", Bull. Am. Phys. Soc. 32 (3), 607 (1987).

[26] H. Hirai, K. Kondo and T. Ohwada, "Diamond Synthesis by Shock Compression from a Thin Graphite Plate with Suppressed Graphitisation", Carbon 33, 203 (1995).

[27] G. Galli *et al.*, "Melting of Diamond at High Pressure", Science 250, 1547 (1990).

[28] G. Galli *et al.*, "Carbon: The Nature of the Liquid State", Phys. Rev. Lett. 63 (9), 988 (1989).

[29] S. Scandolo *et al.*, "Pressure-Induced Transformation Path of Graphite to Diamond", Phys. Rev. Lett. 74, 4015 (1995).

[30] T. Sekine, "An Evaluation of the Equation of State of Liquid Carbon at Very High Pressure", Carbon 31, 227 (1993).

[31] J. Heremans *et al.*, "Observations of Metallic Conductivity in Liquid Carbon", Phys. Rev. Lett. 60 (5), 452 (1988).

[32] M. van Thiel and F.H. Ree, "Multiphase Carbon and its Properties at Complex Mixtures", High Temp.-Press. 24, 195 (1992).

[33] M. Eto, T. Oku and T. Konishi, "High Temperature Young's Modulus of a Fine-Grained Nuclear Graphite Oxidised or Prestressed to Various Levels", Carbon 29, 11 (1991).

[34] F. Durand *et al.*, "Characterisation of the High Temperature Mechanical Behaviour of Carbon Materials", Carbon 32, 857 (1994).

[35] T. Log, J. Melas and B. Larsen, "Technique for Determining Thermal Shock Resistance of Carbon Materials", Carbon 31, 931 (1993).

[36] W.B. Gauster and I.J.Fritz, "Pressure and Temperature Dependences of the Elastic Constants of Compression-Annealed Pyrolitic Graphite", J. Appl. Phys. 45 (8), 3309 (1974).

[37] P. Sievers, "Elastic Stress Waves in Matter Due to Rapid Heating by an Intense High-Energy Particle Beam", CERN LAB.II/BT/74–2, Prévessin (June 1974).

[38] L. Landau and E. Lifszic, "Theory of elasticity", Nauka *(Russian edition)*, Moscow (1965).

[39] International Nuclear Safety Center, Materials and Properties Database, "Recommended Graphite Enthalpy Increments and Heat Capacities", Argonne Nat. Lab./US-DOE Internet documentation, http://www.ra.anl.gov/INSP/matprop

[40] Swanson Analysis Systems, *Inc.*, "ANSYS (Revision 5.2)", SASI/DN-P511:51, Houston, USA (Sept. 30, 1994).

[41] A. Fassò, A. Ferrari, J. Ranft and P.R. Sala, "FLUKA: Present Status and Future Developments", in *Proc. of the IV Int. Conf. on Calorimetry in High Energy Physics*, La Biodola (Is. d'Elba), Italy (Sept. 20–25 1993); Ed. A. Menzione and A. Scribano, World Scientific, p. 493.

[42] J.M. Zazula, "From Particle Cascade Simulations (FLUKA) to Finite Element Heat Transfer and Structural Deformation Analyses (ANSYS)", presented at the *SARE'95 Workshop on Simulating Accelerator Radiation Environment*, CERN-Prévessin, France (October 9-11, 1995); CERN SL/95–93 (BT), Geneva (October 1995).